Turkish Journal of Electrical Engineering & Computer Sciences

http://journals.tubitak.gov.tr/elektrik/

Research Article

Turk J Elec Eng & Comp Sci
(2019) 27: 2309 – 2320

doi:10.3906/elk-1807-195

Vibration analysis of a novel magnetic-viscous nonlinear passive isolator via finite element simulation

Ahmet MERAM*, **Ümit ÖNEN**

Department of Mechatronics Engineering, Faculty of Engineering and Architecture, Necmettin Erbakan University, Konya, Turkey

Received: 18.07.2018 • **Accepted/Published Online:** 29.03.2019 • **Final Version:** 15.05.2019

Abstract: In this paper, the design and the finite element simulation of a novel magnetic-viscous vibration isolator have been presented. The proposed isolator consists of permanent magnets axially aligned in repulsion position and a viscous damper in parallel with them. The nonlinear spring characteristic of the permanent magnets provides a good damping property with this configuration. Explicit finite element analyses have been conducted to examine the dynamic behavior of the isolator. Output displacements and transmissibility ratios were measured for various magnet configurations, dashpot coefficients, and input displacement excitation frequencies to determine the best damping properties. The results of the finite element modeling revealed that the performance of the isolator is highly sensitive to the quantity of magnets. Isolators with four or more magnets can successfully reduce the output displacement. The results indicate that the isolator significantly reduces the displacement transmissibility in frequencies over the resonant frequency region. It is possible to ensure an infinite operating life for magnet-viscous vibration isolators by protecting the magnets against breakage.

Key words: Permanent magnet, nonlinear spring, vibration isolator, vibration analysis, finite element modeling

1. Introduction

Vibration isolators are used to minimize the level of vibrations transmitted to a system from vibration sources. There are many parameters that affect the performance of vibration isolators. The parameters affecting the shock and vibration isolators are not inherently linear, but in order to facilitate the design and analysis process, these parameters are assumed linear in most studies. Many researchers have investigated the design criteria and indices of vibration isolators analytically and experimentally. For instance, Soliman and Ismailzadeh optimized the values of mass, stiffness, and damping ratio of linear isolators [1]. Snowdon reviewed the static and dynamic parameters affecting linear vibration isolators [2]. The linear vibration isolator alleviates transmitted vibrations with an excitation frequency higher than the value of $\sqrt{2}\omega_n$, where ω_n is the undamped natural frequency of the isolator. At frequencies higher than $\sqrt{2}\omega_n$, the transmitted displacement or force becomes smaller than the excitation displacement or force. By reducing the natural frequency and damping ratio of an isolator, the performance of isolator can be improved [3].

Recently, studies on isolators with nonlinear parameters have increased. A comprehensive review on the recent advances in nonlinear vibration isolators was reported in [3]. In nonlinear isolators, the transmissibility depends on the stiffness of the isolator [4]. The soft stiffness may increase the effectiveness of the isolator by

*Correspondence: ameran@erbakan.edu.tr

reducing the resonant frequency. Ravindra and Mallik reported that a soft nonlinear isolator has advantages over those with hard nonlinearity [5]. Nonlinear damping significantly shifts the resonant frequency towards a lesser value compared with linear damping. Kirk investigated the effect of three various types of nonlinear springs on the performance of linear damping isolators exposed to steady random white noise [6]. It was found that the cubic soft spring was effective in reducing transmitted vibrations in limited values. Peng et al. investigated the passive vibration properties of isolators with cubic damping and showed that cubic linear or nonlinear damping can sufficiently decrease the force and displacement transmissibility over the resonance zone [7]. In industrial applications elastomeric isolators, rubbers, and viscous isolators are widely employed. Mallik et al. experimentally investigated the damping and restoring characteristics of elastomeric isolators [8]. Richards and Singh characterized the nonlinear parameters of rubber isolators [9]. They proved that rubber isolators possess nonlinear damping and nonlinear stiffness properties. Carrillo et al. studied a passive isolator consisting of two oblique springs acting in parallel to a vertical spring [10]. Zhou and Liu developed a tunable electromagnetic vibration isolator consisting of a mechanical spring in parallel with a magnetic spring [11]. They experimentally showed that the tuning strategy can guarantee the best performance when the exciting frequency alters or external distortions occur. Liao et al. investigated a vibration isolator consisting of magnetorheological elastomers and they significantly decreased the transmissibility of the payload near the resonant frequency region [12]. Xu et al. theoretically and experimentally analyzed a nonlinear magnetic vibration isolator [13]. They compared the performance of their system with standard linear isolators in low frequency field and showed the excels. Magnetic spring with negative stiffness can be used to create isolation systems with high static and low dynamic stiffness. Wu et al. demonstrated that combining a vibration isolator in parallel with a magnetic spring with negative stiffness can reduce the natural frequency of the isolator [14]. Mofidian and Bardaweel investigated vibration isolation systems consisting of a mechanical oblique spring with geometric nonlinear negative stiffness and a magnetic spring with positive nonlinear stiffness [15]. Also, there is a reported study on vibration isolation systems combining elastic and magnetic springs and viscous and magnetic damping [16]. Nammari et al. conducted a study on a vibration energy harvester with a nonresonant magnetomechanical system [17]. Xu et al. designed a nonlinear magnetic low-frequency vibration isolator with quasizero stiffness [18]. Bo et al. employed magnetic repulsive force and magnetic attractive force effects to design a novel passive nonlinear isolator [19]. Mofidian and Bardaweel used the elastic and magnetic component to design a dual purpose vibration isolator energy harvester device for low-frequency operations [20]. Carrella et al. utilized the negative stiffness of permanent magnets to improve the behavior of a linear passive vibration isolator [21]. There are also studies concerning quasizero-stiffness vibration isolators [22], and high static with low dynamic stiffness nonlinear [23] and multidimensional vibration isolators [24]. Permanent magnets, by generating constant flux sources, can be used to produce passive systems, which operate without external power sources. Permanent magnets are used for very diverse applications including nuclear magnetic resonance imaging, magnetic holding systems, loudspeaker-type actuators, and ABS sensors. Permanent magnets can produce repulsive forces that are much larger than their own weight. Magnetic bearings, which are used in gas centrifuge systems and turbo-molecular pumps, are among the repulsion applications of permanent magnets. Repulsive force systems are also widely used in industry to transmit torque across impenetrable walls [25].

In this study, it was aimed to design a vibration isolator by employing the repulsive force of permanent magnets. The commercial finite element (FE) software Abaqus 6.10 was used to analyze the dynamic behavior of the magnetic-viscous vibration isolator with various configurations and excitation inputs. The repulsive force

between the same poles of two disc magnets was modeled as a transitional nonlinear elastic axial connector. It is supposed to use neodymium disc magnets, which are a combination of neodymium, iron, and boron. Their repulsive force with respect to distance data was obtained from the website of the manufacturer. In the literature there is no study focused on the analysis of a vibration isolator combining permanent magnets in parallel with a viscous damper. Motivated by this fact, this study was initiated to investigate the characteristic performance of the magnetic-viscous vibration isolator.

2. Repulsive force of permanent magnets

A permanent magnet bar produces a magnetic field around its poles as shown in Figure 1.

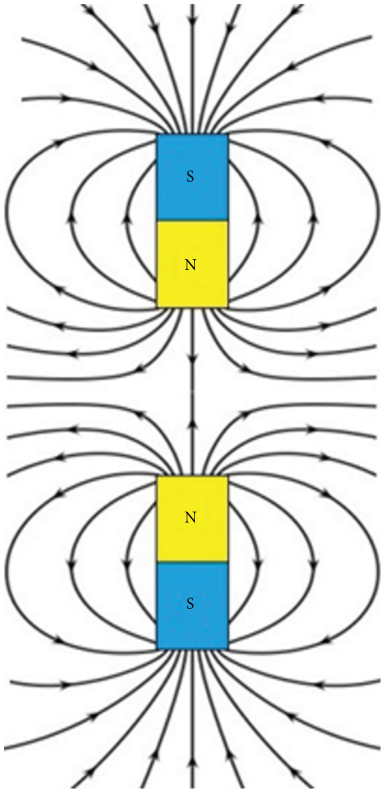

Figure 1. Magnetic field around the poles of permanent magnets in repulsive position.

The repulsive force between two magnets depends on the orientation, magnetization, shape, and distance of the magnets [26]. The force for two similar cylindrical magnets aligned with their axes with radius R and height h may be obtained (at a distance larger than the radius of the magnets) by Eq. (1) [27]:

$$F(x) = \frac{\pi\mu_0}{4} M^2 R^4 [\frac{1}{x^2} + \frac{1}{(x+2h)^2} - \frac{2}{(x+h)^2}], \tag{1}$$

where x is the distance between magnets and M is the magnetization of them. μ_0 is the permeability of space, which is equal to $4\pi \times 10^{-7}\, Tm/A$. For small values of x, the results are inaccurate since the force becomes large for close-to-zero distances. In this study, a neodymium, N45, nickel-plated disc magnet is used. The specifications of the permanent magnet are given in the Table.

Table. Dimensions,types and specifications of cylindrical magnet.

Magnet type	Diameter [mm]	Height [mm]	Residual magnetism [Gauss]	Coercive field strength [kA/m]
N45	45	30	13200–13700	860–995

The repulsive force vs. distance curve for the neodymium, N45, nickel-plated disc magnet is shown in Figure 2. There is a combination of linear and nonlinear relationships between the repulsive force and distance of two identical cylindrical magnets [20]. When the distance between two magnets is close to 50 mm, the repulsive force is approximately zero. The force vs. distance curve shows linear behavior until the distance reaches about 15 mm. In distances between 15 mm and contact position, the force vs. distance relationship is nonlinear and the force increases sharply. The repulsive force between two magnets acts as a nonlinear spring element. The pushing force on the spring is zero as the distance between two magnets is large enough (in this study, approximately 50 mm). By bringing two magnets close to each other, the pushing force is increased to about 800 N.

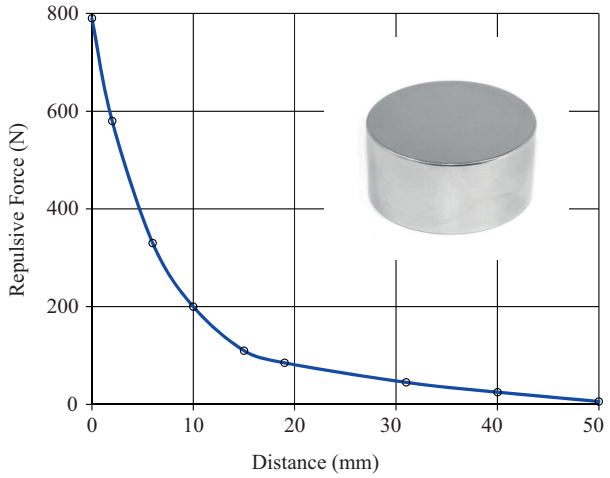

Figure 2. The repulsive force vs. distance curve for N45 nickel-plated disc magnet (S-45-30-N).

3. Design of vibration isolator with a nonlinear magnetic spring

In order to design the vibration isolator, a disc permanent magnet was fixed at the bottom of a tube and other magnets were dropped at the tube. The identical disc magnets were placed end to end in a vertical tube in a repelling configuration. For dissipating the vibration energy, a viscous damper was located parallel to the magnet housing. Figure 3 shows the vibration isolator with five magnets.

3.1. Lumped mass-spring model of vibration isolator

The lumped mass-spring models of the isolator with two, three, four, and five magnets are shown in Figure 4. When the magnets are placed at nearly 50 mm distance from each other, they compensate their weight and stay stable. In this position, the repulsive force of the magnets acts as a nonlinear spring.

The governing constitutive equations for the spring and viscous dashpot are presented here. A viscous damping is a force that is proportional to the velocity of the mass and opposes its motion. Applying Newton's

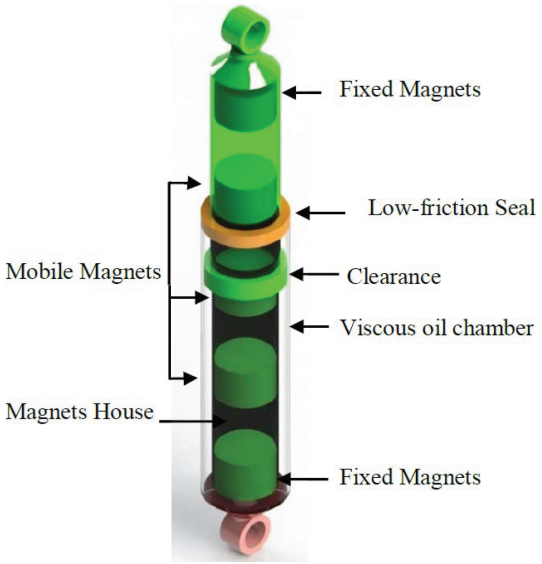

Figure 3. Magnet-viscous vibration isolator.

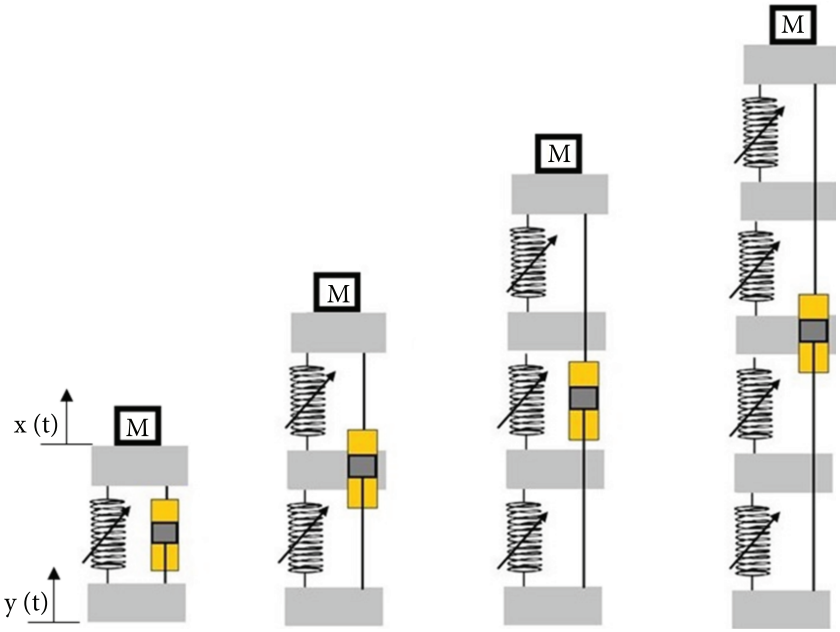

Figure 4. Lumped mass-spring models of vibration isolator with two, three, four, and five magnets.

second law, the equation of motion can be written as follows:

$$\sum F_y = \alpha(y-x) + \beta(y-x)^3 - c(\dot{x}-\dot{y}) = m\ddot{x}. \tag{2}$$

The values of α, β, and γ are determined from the relation between the repulsive force and the distance of the magnets. For $y = Y\sin(\omega t)$,

$$m\ddot{x} = \alpha(Y\sin(\omega t) - x) + \beta(Y\sin(\omega t) - x)^3 - c(\dot{x} - Y\omega\cos(\omega t)). \tag{3}$$

In order to solve the nonlinear high-order differential equation presented in Eq. (3), various techniques such as harmonic balance and Taylor expansion methods can be employed [15, 19, 28]. The acceleration at the initial point can be written as follows:

$$\ddot{x}(0) = [\alpha(Y\sin(0) - x(0)) + \beta(Y\sin(0) - x(0))^3 - c(\dot{x}(0) - Y\omega\cos(0))]/m. \tag{4}$$

In order to obtain the approximate displacement function at time $t + \Delta t$, the Taylor series expansion up to the third term may be used:

$$x(t + \Delta t) = x(t) + \dot{x}(t)\Delta t + \frac{1}{2}\ddot{x}(t)\Delta t^2. \tag{5}$$

Backward difference approximation can be used to obtain the approximate velocity function at time $t + \Delta t$:

$$\dot{x}(t + \Delta t) = \frac{x(t + \Delta t) - x(t)}{\Delta t}. \tag{6}$$

Then Eq. (3) used to obtain the approximate acceleration function at time $t + \Delta t$:

$$\ddot{x}(t+\Delta t) = [\alpha(Y\sin(t+\Delta t) - x(t+\Delta t)) + \beta(Y\sin(t+\Delta t) - x(t+\Delta t))^3 - c(\dot{x})(t+\Delta t) - Y\omega\cos(t+\Delta t))]/m. \tag{7}$$

The first iteration can be written as follows:

$$x(\Delta t) = x(0) + \dot{x}(0)\Delta t + \frac{1}{2}\ddot{x}(0)\Delta t^2, \tag{8}$$

$$\dot{x}(\Delta t) = \frac{x(\Delta t - x(0))}{\Delta t}, \tag{9}$$

$$\ddot{x}(\Delta t) = [\alpha(Y\sin(\Delta t) - x(\Delta t)) + \beta(Y\sin(\Delta t) - x(\Delta t))^3 - c(\dot{x}(\Delta t) - Y\omega\cos(\Delta t))]/m. \tag{10}$$

The reiteration formula can be expressed as follows:

$$x_n = x_{n-1} + \dot{x}_{n-1} + \frac{1}{2}\ddot{x}_{n-1}\Delta t^2, \tag{11}$$

$$\dot{x}_{n-1} = (x_n - x_{n-1})/\Delta t, \tag{12}$$

$$\ddot{x}_n = [\alpha(Y\sin((n-1)\Delta t) - x_{n-1}) + \beta((Y\sin(n-1)\Delta t) - x_{n-1})^3 - c(\dot{x}_{n-1} - Y\omega\cos((n-1)\Delta t))]/m. \tag{13}$$

The harmonic balance method (HBM) is used to obtain the displacement transmissibility. The relative displacement between the mass and the base defined as $z = x - y$ and the motion excitatition defined as $y = Y_0 sin(\omega t - \varphi)$ are used to rewrite the equation of motion given in Eq. (2):

$$\ddot{z} + \frac{\alpha}{m}z + \frac{\beta}{m}z^3 + \frac{c}{m}\dot{z} = Y_0\omega^2 sin\omega t. \tag{14}$$

By introducing the following nondimensional parameters,

$$\omega_n = \sqrt{\frac{\alpha}{m}} \qquad \lambda = \frac{\omega}{\omega_n} \qquad \tau = \omega_n t, \qquad \gamma = \frac{\beta}{m} \qquad \delta = z, \qquad \dot{\delta} = \frac{\dot{z}}{\omega_n}, \qquad \ddot{\delta} = \frac{\ddot{z}}{{\omega_n}^2}, \qquad \xi = \frac{c}{2m\omega_n},$$

Eq. (14) takes the form given below:

$$\ddot{\delta} + 2\xi\dot{\delta} + \delta + \gamma\delta^3 = Y_0\lambda^2 sin(\lambda\tau - \varphi). \tag{15}$$

The first approximation to the steady-state solution of Eq. (15) based on the HBM [15, 19, 29] is assumed in the following form:

$$\delta = Dsin\lambda\tau, \tag{16}$$

$$-D\lambda^2 sin(\lambda\tau) + 2\xi D\lambda cos(\lambda\tau) + Dsin(\lambda\tau) + \lambda D^3 sin^3(\lambda\tau) \quad = \quad Y_0\lambda^2 sin(\lambda\tau - \varphi). \tag{17}$$

The following trigonometric relation is applied on the first harmonic term that is taken:

$$sin^3(\lambda\tau) = \left(\frac{-sin(3\lambda\tau)}{4} + \frac{3sin(\lambda\tau)}{4}\right) = \frac{3}{4}sin(\lambda\tau), \tag{18}$$

$$-D\lambda^2 + D + \frac{3}{4}\gamma D^3 = Y_0\lambda^2 cos\varphi, \tag{19}$$

$$2\xi D\lambda = -Y_0\lambda^2 sin\varphi, \tag{20}$$

$$[-D\lambda^2 + D + \frac{3}{4}\gamma D^3]^2 + 4\xi^2 D^2\lambda^2 = {Y_0}^2\lambda^4. \tag{21}$$

By substituting Eq. (18) into Eq. (17) and equating the coefficient of $sin(\lambda\tau)$ and $cos(\lambda\tau)$,

$$D^2[-\lambda^2 + 1 + \frac{3}{4}\gamma D^2]^2 + 4\xi^2 D^2\lambda^2 = {Y_0}^2\lambda^4. \tag{22}$$

The displacement transmissibility is thus defined as:

$$TR = \frac{D}{Y_0} = \frac{\lambda^2}{\sqrt{(-\lambda^2 + 1 + \frac{3}{4}\gamma D^2)^2 + (4\xi^2\lambda^2)}}. \tag{23}$$

3.2. Finite element modeling

In order to generate the FE model, the geometrical model was drawn as shown in Figure 3. Then each part depending on its structural properties was meshed and an element type was assigned. A three-dimensional connector element (CONN3D2) was used to analyze the nonlinear spring behavior of the permanent magnet repulsive force. This element has two nodes with six degrees of freedom (DOF) in each node. The connector element imposes kinematic constraints in the model. In the interaction module, point-to-point wire features were used to define connector geometry. In the present model, the connector elements are placed between the

reference points of permanent magnets. Nonlinear elastic behavior is assigned to the transitional type axial connector. The transitional basic connection components affect transitional DOFs at both nodes. For nonlinear elasticity, force has been defined as a nonlinear function of relative displacement.

In order to simulate the viscous damping of system, dashpot elements known as DASHPOTA were utilized. The dashpot coefficient depends on the viscosity properties of oil, orifice, or clearance geometric configurations. The dashpot clearance and orifice produce a constant damping coefficient and variable damping, respectively. In this study a constant dashpot coefficient was used. The damping forces and stationary and nonstationary parts of the model and also the magnets are defined as a rigid body. The mass of the parts is assigned to their reference points. Penalty tangential contact properties are defined between the motional parts. Dynamic/explicit analysis with user-defined increment time, 0.0001 s, has been conducted. The stable increment time has been specified by considering dashpot coefficient and spring stiffness. By considering the repulsive force capacity of each magnet as approximately 80 kg, the isolator has been examined with 5 kg mass. Analysis is performed in two steps. In the first step, the sprung mass ($m = 5$ kg) is added to the head of the isolator and analysis is carried out to obtain the equilibrium position of the magnets. In the second step, sinusoidal displacement excitation inputs with different frequency spectra are assigned to the base of the isolator as the boundary condition. The displacement excitation is defined by Eq. (11). The amplitude of the excitation signal is 50 mm.

4. Results and discussion

In this section, the results of the finite element simulation of a magnetic-viscous vibration isolator are presented. First of all, analysis was conducted to measure the spring stiffness of vibration isolators without a viscous damper. Then, under the sinusoidal displacement excitation given in Eq. (24), the effect of the number of magnets on the dynamic behavior of the vibration isolator was analyzed. It was found that the quantity of magnets is effective on the performance of the isolator. When the quantity of magnets is lower than four, the output displacement becomes lager than the input. Therefore, to measure the effect of the excitation frequency and dashpot coefficient on the output displacement and transmissibility, analyses were conducted on the isolator consisting of five magnets. The displacement excitations for various frequencies are shown in Figure 5. The program reads the results in the first step and propagates the boundary conditions. The program calculates the nodal displacement, velocity, acceleration, and reaction forces of the model:

$$y = 50\sin(\omega t), \qquad 0 \le t \le \frac{\pi}{\omega}. \tag{24}$$

In order to examine the accuracy of the FE simulation of vibration, it is essential to establish the energy balance in the simulation [30]. The energy balance equation expressed by Eq. (15) was utilized in the vibration isolator simulation:

$$E_I + E_{KE} + E_{FD} + E_V - E_{SW} = E_{TOT}, \tag{25}$$

where E_I is the internal energy and includes the recoverable elastic strain energy, and E_KE is the kinetic energy. E_{FD} is the dissipated frictional energy. E_V is the dissipated viscous energy. E_{SW} is the total of the work accomplished by the external loads. E_{TOT} is the sum of all energy components. In FE explicit simulation, if E_{TOT} is almost constant, the value of the total error is normally smaller than 1%. The verification of the energy balance in vibration simulation showed that the total energy remained constant.

4.1. Nonlinear spring stiffness

In order to determine the stiffness of the isolator, the DOF of the base is restricted in all directions. An input displacement is applied to the head of the isolator under quasistatic conditions. The reaction force is measured from the base of the isolator. The reaction force vs. displacement curves with respect to the magnets of the isolators are given in Figure 6. It is observed that the force vs. displacement curves of isolators consist of two distinguishable linear and nonlinear regions. The linear behavior at the start follows a nonlinear manner. By increasing the number of magnets, the linear region becomes larger. It can be concluded that by adding more magnets, it is possible to produce a spring with soft stiffness.

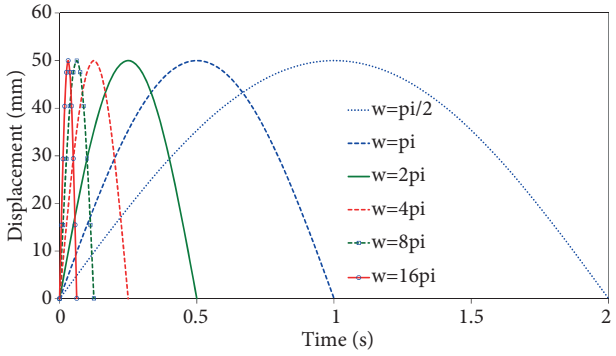

Figure 5. Displacement excitation inputs for various frequencies.

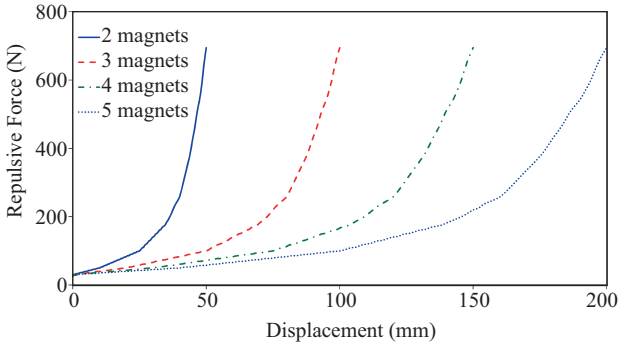

Figure 6. The reaction forces vs. displacements of isolator.

4.2. Effect of quantity of magnets on output displacement

In order to evaluate the effect of quantity of magnets on output displacement of the vibration isolator, numerical analysis was conducted. A sprung mass with m =5 kg was added to the top of the isolator. The dashpot coefficient of the viscous damping was assumed to be c = 0.01 Ns/mm. The displacement excitation with 16π Hz frequency as shown in Figure 5 was applied to the base of the isolator. The output displacement of the sprung mass was measured for isolators consisting of two, three, four, and five serially arranged permanent magnets. Figure 7 shows the displacement vs. time. It is observed that the output displacement in isolators with two and three magnets is larger than the excitation displacement. Therefore, the isolators with fewer than four magnet are not beneficial for vibration isolation with sprung mass, dashpot coefficient, and excitation frequency as tested in this study. The output displacements in the isolators with four and five magnets are smaller than the input displacements. Also, as the number of magnets increased from four to five, the transmissibility was improved. The transmissibility of 0.8 in the isolator with four magnets is reduced to 0.5 in the isolator with five magnets.

4.3. Effect of excitation frequency on output displacement and damping

The excitation frequency spectrum is among the other parameters that influence the performance of a vibration isolator. In order to evaluate the performance of the isolator in various excitation frequencies, sinusoidal displacement excitation inputs as shown in Figure 5 are given to the base of the isolator. The displacements of the sprung mass with respect to time are shown in Figures 8–10, which were measured for the frequencies between π and 16π for dashpot coefficients c = 0.01, 0.03, and 0.06 Ns/mm, respectively. By analysis of the measured data, it was found that the resonance may happen around $\omega = 2\pi$. Increasing the excitation

frequency from $\omega = 2\pi$, the output displacement is decreasing. In frequencies over 8π, the output displacement is smaller than the input one. In comparison to other excitation frequencies, the vibration is damped better by the $\omega = 16\pi$ frequency.

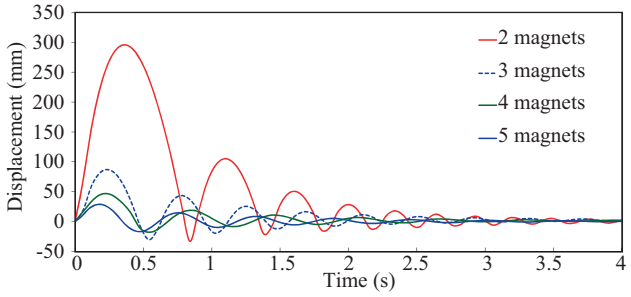

Figure 7. Displacement of the sprung mass vs. time with respect to the number of magnets in isolator.

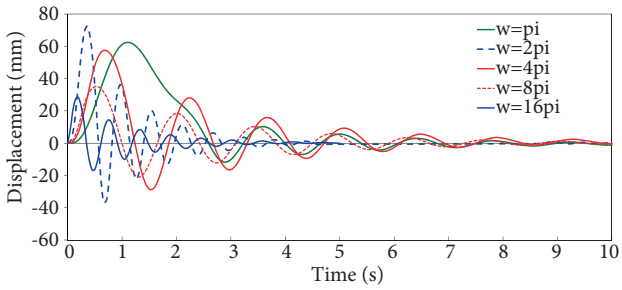

Figure 8. Displacement vs. time of the sprung mass for $c = 0.01$ Ns/mm.

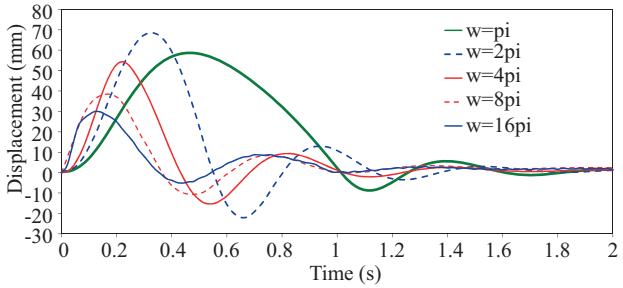

Figure 9. Displacement vs. time of the sprung mass for $c = 0.03$ Ns/mm.

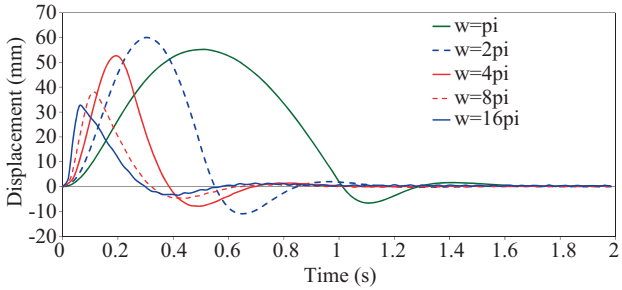

Figure 10. Displacement vs. time of the sprung mass for $c = 0.06$ Ns/mm.

4.4. Effect of viscous damping on transmissibility

In order to investigate the effect of viscous damping on displacement transmissibility, transmissibility ratio (TR) values are extracted by using displacement vs. time curves of the sprung mass as shown in Figure 11. The output displacement values presented in Figures 8–10 are used to calculate the TR. It is observed for the frequencies over the resonant region that the isolation can be improved by increasing the dashpot coefficient. In frequencies below the resonant region, the effect of the damping ratio on the TR is negligible.

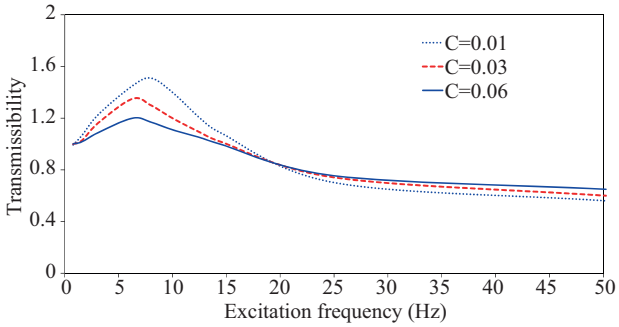

Figure 11. Displacement transmissibility ratio (TR) vs. excitation frequency.

5. Conclusion

In this study, the repulsive force of permanent magnets combined with a viscous damper was employed to design a novel vibration isolator. The FE method has been utilized to measure the stiffness of the magnetic isolator. The effects of the quantity of magnets and excitation frequency and dashpot coefficient on the output displacement, damping, and transmissibility were also investigated numerically. The numerical simulation results revealed that by increasing the number of magnets in repulsion position, it is possible to obtain a spring with soft elastic stiffness, which is beneficial to acquire low transmissibility over a wide frequency range. The quantity of the magnets in the vibration isolator is effective in reducing the output displacement of the sprung mass. In high frequencies, as the number of magnets increased, the output displacement was decreased. When the dashpot coefficient is increased, the damping is improved and the output displacement is decreased. In frequencies below the resonant region, the effect of damping ratio on TR is negligible. Finally, the vibration isolation performance of the magnetic-viscous isolator was tested numerically. It was proved that the isolator operates properly. In future studies, the prototype of the vibration isolator will be fabricated and experimentally tested.

Acknowledgment

We would like to thank Prof Dr Ata Muğan from İstanbul Technical University for his valuable support in finite element simulations.

References

[1] Soliman JI, Ismailzadeh E. Optimization of unidirectional viscous damped vibration isolation system. Journal of Sound and Vibration 1974; 36 (4): 527-539.

[2] Snowdon JC. Vibration isolation use and characterization. Journal of the Acoustical Society of America 1979; 66: 1245-1279.

[3] Ibrahim RA. Recent advances in nonlinear passive vibration isolators. Journal of Sound and Vibration 2008; 314 (3-5): 371–452.

[4] Kolovsky MZ. Nonlinear Dynamics of Active and Passive Systems of Vibration Protection. Berlin, Germany: Springer, 1999.

[5] Ravindra B, Mallik AK. Performance of nonlinear vibration isolators under harmonic excitation. Journal of Sound and Vibration 1994; 170: 325-337.

[6] Kirk CL. Nonlinear random vibration isolators. Journal of Sound and Vibration 1988; 124: 157-182.

[7] Peng ZK, Meng G, Lang ZQ, Zhang WM, Chu FL. Study of the effects of cubic nonlinear damping on vibration isolations using harmonic balance method. International Journal of Non-Linear Mechanics 2012; 47 (10): 1073-1080.

[8] Mallik AK, Kher V, Puri M, Hatwal H. On the modeling of non-linear elastomeric vibration isolators. Journal of Sound and Vibration 1999; 219; 239-253.

[9] Richards CM, Singh R. Characterization of rubber isolator nonlinearities in the context of single and multi-degree-of-freedom experimental systems. Journal of Sound and Vibration 2001; 247 (5): 807-834.

[10] Carrella A, Brennan MJ, Waters TP. Analysis of a passive vibration isolator with quasi-zero-stiffness characteristic. Journal of Sound and Vibration 2007; 301 (3-5): 678-689.

[11] Zhou N, Liu K. A tunable high-static-low-dynamic stiffness vibration isolator. Journal of Sound and Vibration 2010; 329 (9): 1254-1273.

[12] Liao GJ, Gong XL, Xuan SH, Kang CJ, Zong LH. Development of a real-time tunable stiffness and damping vibration isolator based on magnetorheological elastomer. Journal of Intelligent Material Systems and Structures 2012; 23 (1): 25-33.

[13] Xu D, Yu Q, Zhou J, Bishop SR. Theoretical and experimental analyses of a nonlinear magnetic vibration isolator with quasi-zero-stiffness characteristic. Journal of Sound and Vibration 2013; 332 (14): 3377-3389.

[14] Wu W, Chen X, Shan Y. Analysis and experiment of a vibration isolator using a novel magnetic spring with negative stiffness. Journal of Sound and Vibration 2014; 333 (13): 2958-2970.

[15] Mofidian SMM, Bardaweel H. Displacement transmissibility evaluation of vibration isolation system employing nonlinear-damping and nonlinear-stiffness elements. Journal of Vibration and Control 2018; 24 (18): 4247-4259.

[16] Mofidian SMM, Bardaweel H. Theoretical study and experimental identification of elastic-magnetic vibration isolation system. Journal of Intelligent Material Systems and Structures 2018; 29 (18): 3550-3561.

[17] Nammari A, Caskey L, Negrete J, Bardaweel H. Fabrication and characterization of non-resonant magneto-mechanical low-frequency vibration energy harvester. Mechanical Systems and Signal Processing 2018; 102: 298-311.

[18] Xu D, Yu Q, Zhou J, Bishop SR. Theoretical and experimental analyses of a nonlinear magnetic vibration isolator with quasi-zero-stiffness characteristic. Journal of Sound and Vibration 2013; 332 (14): 3377-3389.

[19] Yan B, Ma H, Zhao C, Wu C, Wang K et al. A vari-stiffness nonlinear isolator with magnetic effects: Theoretical modeling and experimental verification. International Journal of Mechanical Sciences 2018; 148: 745-755.

[20] Mofidian SMM, Bardawell H. A dual-purpose vibration isolator energy harvester: experimental model. Mechanical Systems and Signal Processing 2019; 118: 360-376.

[21] Carrella A, Brennan MJ, Waters TP, Shin K. On the design of a high-static-low-dynamic stiffness isolator using linear mechanical springs and magnets. Journal of Sound and Vibration 2008; 315 (3): 712-720.

[22] Sun X, Xu J, Jing X, Cheng L. Beneficial performance of a quasi-zero-stiffness vibration isolator with time-delayed active control. International Journal of Mechanical Sciences 2014; 82: 32-40.

[23] Sun X, Jing X. A nonlinear vibration isolator achieving high-static-low-dynamic stiffness and tunable anti-resonance frequency band. Mechanical Systems and Signal Processing 2016; 80: 166–188.

[24] Li B, Zhao W, Deng Z. Modeling and analysis of a multi-dimensional vibration isolator based on the parallel mechanism. Journal of Manufacturing Systems 2012; 31 (1): 50–58.

[25] Lacheisserie T, Gignoux D, Schlenker M. Magnetism: Materials and Applications. Berlin, Germany: Springer Science & Business Media, 2005.

[26] Jindal UC. Material Science and Metallurgy. Delhi, India: Pearson Education, 2013.

[27] Vokoun D, Beleggia M, Heller L, Sittner P. Magnetostatic interactions and forces between cylindrical permanent magnets. Journal of Magnetism and Magnetic Materials 2009; 321 (22): 3758–3763.

[28] El-Nady AO, Lashin MMA. Approximate solution of nonlinear duffing oscillator using Taylor expansion. Journal of Mechanical Engineering and Automation 2016; 6 (5): 110-116.

[29] Abdur Razzak M. A simple harmonic balance method for solving strongly nonlinear oscillators. Journal of the Association of Arab Universities for Basic and Applied Sciences 2016; 21: 68-76.

[30] Meran AP, Baykasoglu C, Mugan A, Toprak T. Development of a design for a crash energy management system for use in a railway passenger car. Proceedings of the Institution of Mechanical Engineers Part F 2016; 230 (1): 206–219.